



Silver doped silica-methyl hybrid coatings. Structural evolution and antibacterial properties



R.A. Procaccini^{a,*}, C.A. Studdert^b, S.A. Pellice^a

^a Instituto de Investigación en Ciencia y Tecnología de Materiales (INTEMA), UNMdP-CONICET., Av. Juan B. Justo 4302, 7600 Mar del Plata, Argentina

^b Instituto de Investigaciones Biológicas (IIB), UNMdP-CONICET., Funes 3250, 7600 Mar del Plata, Argentina

ARTICLE INFO

Article history:

Received 2 April 2013

Accepted in revised form 13 January 2014

Available online 25 January 2014

Keywords:

Silver clusters

Sol-gel

Bactericidal coatings

SAXS

Silver nanoparticles

ABSTRACT

In this work, the effect of silver doping on the organic–inorganic hybrid structure of sol–gel coatings and its performance as bactericidal materials was analyzed. Coatings were synthesized through the hydrolytic condensation of tetraethoxysilane (TEOS) and methyl-triethoxysilane (MTES); silver nitrate was used as a source of Ag⁺ ions. The structural analysis, performed through Small Angle X-ray Scattering (SAXS) with synchrotron light, Fourier Transformed Infrared (FTIR) and UV–visible spectroscopies, revealed the complex scenario developed as the network crosslinking rises during the thermal treatment. The matrix structure works as a size-selective membrane where only the smaller silver clusters and ions are released to the surface while the higher nanoparticles remain trapped inside. Finally, bacteriologic analysis, performed with *Escherichia coli* cultures, confirmed a tight correlation between silver lixiviation and the inhibition halos observed in agar diffusion tests.

© 2014 Elsevier B.V. All rights reserved.

1. Introduction

The development of new functional materials capable to provide an effective biocide activity is an active area of research, given the multiple applications that they can offer. Both in the field of health as for functional purposes, the action of viruses and bacteria often presents serious damages that can turn in economic losses or even in loss of human lives.

From the side of the materials science, the development of new functional materials capable to provide an effective biocide activity is pursued by many research groups around the world. One of the more promising research areas aims to take advantage of the well-known biocide power of silver ions [1–5]. Ag⁺ ions have an effective action against bacteria life inhibiting their DNA replication process, increasing the permeability of the cytoplasmic membrane and inhibiting the respiratory enzymes, causing asphyxia of the bacteria. Thus, silver is currently used as the active additive, against fungus and bacteria, both in medical devices and in commercial textile products, like sportswear and burn bandages [6–9]. Likewise, the use of silver as additive for thin solid coatings could provide a powerful tool in order to set a major obstacle to the spread of infections.

On the other hand, the sol–gel chemistry presents a very versatile way to produce tailored materials and, since early 1990s, it is a world-wide subject of study as a method to produce functional coatings [10]. For that reason, it is a process commonly used to prepare inorganic and organically modified glassy materials by means of hydrolysis and

condensation of silicon alkoxides. The sol–gel method also offers the possibility of incorporation of different compounds and particles resulting in a very versatile approach to produce multifunctional materials. In the case of silver, its ions present a strong tendency to be reduced in the chemical conditions proper of the sol–gel process, resulting in an agglomeration process that carries to a rise of silver nanoparticles. Depending on the environmental conditions that the biocide material will work, i.e., immersed in an aqueous fluidic media or at the air atmosphere, the silver aggregation state should be determinant of its efficiency against microorganisms. If a biocide material, based in metallic silver nanoparticles, is exposed to an aqueous media, a steady Ag⁺ release could be reached from a superficial oxidative process with dissolved oxygen [11]. Moreover, the supply of silver ions should be strongly dependent on its initial availability inside the material and the agglomeration process should be avoided. A useful method to stabilize the silver in the ionic state is by formation of coordination compounds [12]. Even so, the growth of small silver clusters and -nanoparticles is nearly impossible to avoid when the doped sol is applied as a coating and the thermal treatment is performed [13]. This agglomeration process could result in a significant reduction of the biocide effect by entrapment of the silver particles into the sol–gel matrix. A better understanding of the self-arrangement of silver ions and its diffusion process within its surrounding hybrid matrix could shed light on the improvement of the biocide material where the silver content is present in its proper dosage avoiding its incorporation in unnecessary amount.

In order to develop a hybrid organic–inorganic coating providing a controlled silver release rate, avoiding an initial burst release effect and dangerous cytotoxic conditions, both the matrix structure and the agglomeration process of silver should be optimized. In this

* Corresponding author. Tel.: +54 223 4816600; fax: +54 223 4810046.

E-mail address: rprocaccini@fi.mdp.edu.ar (R.A. Procaccini).

work the study of silver agglomeration phenomena inside of a silica-methyl hybrid matrix as a function of the thermal treatment was addressed. The resulting relationship between silver release and bactericidal effect of sol-gel coatings was also studied. Through the use of a synchrotron radiation source, Small Angle X-ray Scattering (SAXS) was performed to analyze the physical structure of the hybrid matrix and the evolution of silver clusters as the temperature of the thermal treatment increases. The whole developed structure was also analyzed by Fourier Transformed Infrared spectroscopy (FTIR) and UV-visible spectroscopy. Correlation between the silver release process and the bactericidal effect of coatings was carried out through the study of lixiviation of silver, followed by X-ray Fluorescence (XRF), and microbiological analysis by agar diffusion tests against *Escherichia coli* cultures.

2. Experimental

2.1. Sample preparation

Hybrid organic-inorganic sols were synthesized by hydrolytic condensation of tetraethoxysilane (TEOS, 98%, Aldrich) methyltriethoxysilane (MTES, 99%, Aldrich) and deionized water in molar ratios $\text{TEOS/MTES} = 36/54$ and $-\text{OCH}_2\text{CH}_3/\text{H}_2\text{O} = 2$. The chemical reaction was acid catalyzed at room temperature using concentrated HNO_3 (0.47% v/v). Synthesis was performed under vigorous stirring, at 1500 rpm, until a homogeneous solution was obtained. Silver doped sol was prepared through the addition of a pyridine (Py) stabilized solution of AgNO_3 and absolute ethanol to the previously synthesized undoped sol, obtaining a colorless and homogeneous doped sol with molar ratios $\text{Py/Ag} = 2/1$ and $\text{Si/Ag} = 97/3$. Through the dip-coating process, at withdrawal speed of 25 cm/min, both doped and undoped homogeneous coatings, called TMAg and TM respectively, were obtained on microscope glass slides. After drying, coatings were exposed to thermal treatments of 50, 100, 150 and 200 °C, in air atmosphere during 30 min.

2.2. Synchrotron SAXS

The structural evolution of the hybrid matrix and silver clusters was analyzed, as a function of the thermal treatment, by Small Angle X-ray Scattering (SAXS). The experiments were carried out using the SAXS1 beamline of the National Laboratory of Synchrotron Light (LNLS, Campinas, Brazil). Coatings were taken out from glass substrates by scratching. The resulting glassy powder was placed in the sample holders by adhesive polyimide film (Kapton®, DuPont). In order to subtract the contribution of the adhesive tape from SAXS patterns, Kapton film was used as background. The collimated beam crossed the samples through an evacuated flight tube and was scattered to 2D bump-bonded hybrid-pixel Pilatus detector with an active area of 28 cm² and pixel size of $172 \times 172 \mu\text{m}^2$. The geometrical configuration was set up with the sample detector distance of 473.5 mm with monochromatic light of $\lambda = 1.55 \text{ \AA}$. The q range was calibrated with silver behenate, which has a well-known lamellar structure with $d = 5.848 \text{ nm}$ [14]. The isotropic 2D scattering patterns were collected after exposure times of 10 s. Images were corrected taking into account the detector dark noise and normalized by the sample transmission considering the 360 azimuthal scan. This procedure was carried out using the FIT2D software [15].

2.3. FTIR

Influence of silver doping on the silica structure was analyzed through Fourier Transformed Infrared Spectroscopy (Nicolet 6700 FTIR Spectrometer, Thermo Electron Corporation) by Attenuated Total Reflectance (ATR). The FTIR spectra were collected for coating films

after synthesis and thermal treatment of the samples was properly finished for each batch.

2.4. UV-visible

The UV-visible absorption spectra were obtained through a double-beam spectrophotometer (Shimadzu UV-160A) scanning the 200–1100 nm spectral range in transmission mode. Powder samples obtained as described for SAXS experiments were placed in sample holders by polypropylene adhesive tape (Scotch® 550, 3 M). In order to subtract the contribution of the adhesive tape from UV-visible spectra, Scotch tape was used as background.

2.5. XRF

Ag-doped coatings were immersed in deionized water at 30 °C, up to 140 h, keeping an immersed surface/water ratio of 0.4 cm²/ml. X-ray Fluorescence Spectroscopy (XRF, MiniPal 2, PANalytical) was performed at 5 kv and 650 μA in He atmosphere. Silver release was determined, as a function of the immersion time and thermal treatment, following the band area corresponding to the electronic transition $L\alpha$ of Ag atoms at 2.982 keV. XRF curve fits were performed by Origin software (OriginPro 8 SR0, v8.0724 (B724), OriginLab Corporation) giving R^2 values between 0.9988 and 0.9993.

2.6. Agar diffusion tests

Overnight cultures of *E. coli* (K12 strain RP437) were diluted 1/50 and spread onto rich medium agar plates, containing 1% tryptone, 0.5% yeast extract, 0.5% NaCl and 1.3% agar. Microscope glass slides with different coatings were placed on the agar surface, and plates were incubated at 37 °C for 24 h. The inhibitory activity was visualized as a clear halo between the glass and the bacterial lawn.

3. Results and discussion

Transparent, homogeneous and colorless sols were synthesized. After dip-coating deposition and thermal treatment at different temperatures in air atmosphere, homogeneous and crack-free coatings were obtained. A light yellowish coloration was observed in silver doped samples treated at 150 °C.

3.1. Effect of thermal treatment and silver doping on the sol-gel hybrid structure

The structure of the silica network of the coatings as a function of the thermal treatment and the presence of silver were analyzed through Fourier Transformed Infrared spectroscopy (FTIR), Fig. 1.

Despite the strong overlapping of the absorption bands, ATR-FTIR spectra reveal some features of the influence of the thermal treatment on the silica network, Fig. 1a. Both the longitudinal optic (LO) and the transversal optic (TO) modes of the asymmetric vibration of Si–O–Si bonds can be usually observed in hybrid sol-gel coatings. The presence of the bands corresponding to the LO mode, at 1130 and 1170 cm^{−1} (sh), is attributed to the porous structure in the silica network [16,17], while the TO bands, around 1020, 1045 and 1100 cm^{−1}, correspond to structural units of isolated cyclosiloxanes or terminal rings, with larger Si–O–Si angles and Si–O bond lengths [18–20]. On the other hand, taking into account that the gel conversion of a pure silica sol, from TEOS in acidic conditions, corresponds to the condensation of at least 80% of the hydrolysable groups [21] and that if a fraction of TEOS (tetrafunctional) is replaced by a trifunctional alkoxyde (MTES) the gel conversion should be even higher [22] the contribution of the bands of residual alkoxyde groups, that do not become into a Si–O–Si bond nor to a Si–OH group, should be strongly overlapped by the corresponding ones of the silica network of the gelled and thermally

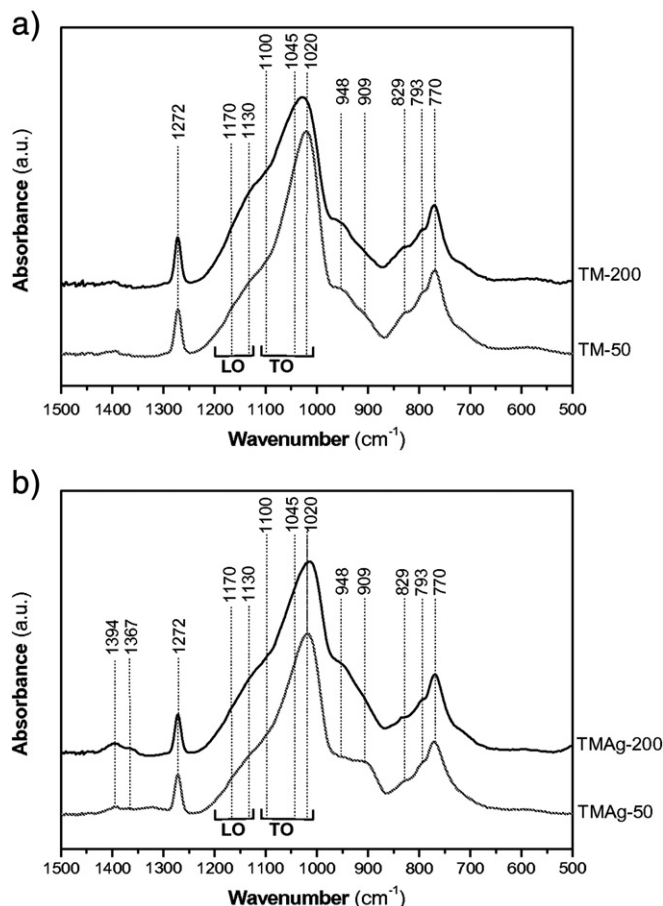


Fig. 1. FTIR spectra of a) TM and b) TMAg coatings treated at 50 and 200 °C in air atmosphere.

treated films [13]. Therefore, the bands at 770 and 793 cm^{-1} can be certainly attributed to the symmetric stretching of the Si–O–Si bonds [23,24]. The methyl groups, supplied by MTES, are observed through its bands at 829 and 1272 cm^{-1} , which are attributed respectively to the $\nu(\text{Si}-\text{C})$ and $\delta_s(\text{CH}_3)$ [25]. As might be expected, the treatment of silver-free coatings at higher temperatures (sample TM-200) was accompanied by an increase of the LO bands in detriment of the TO ones whose maximum, besides a widening, undergoes a shift from 1020 to 1028 cm^{-1} . Since no significant changes were observed in the bands corresponding to Si–OH bonds and non-bridging oxygen, Si–O $^-$, [26,27] at 948 and 909 cm^{-1} respectively, besides a higher crosslinking of the silica network, this fact could be explained by the incorporation of the isolated cyclosiloxanes and smaller silica clusters, observed at 1020 cm^{-1} , to the hybrid matrix.

The FTIR spectra of silver doped samples TMAg-50 and TMAg-200 are shown in Fig. 1b. Addition of silver nitrate to the sol–gel matrix did not introduce any significant change in the silica network when it was dried at 50 °C; both symmetrical and asymmetrical vibration modes of silica are clearly similar between samples TM-50 and TMAg-50 (Fig. 1a). On the other hand, silver nitrate induced a strong increase around the band at 909 cm^{-1} . This band, related to the presence of non-bridging oxygen, can be undoubtedly attributed to the presence of silver in the silica structure. De et al. [28] reported, in silver doped sol–gel silica coatings, a band at 883 cm^{-1} attributed to terminal Si–O $^-$ groups arising from a Si–O–Ag network. Silver nitrate has a broad band at the 1310–1320 cm^{-1} region corresponding to the equilibrium of the $\text{NO}_3^- \text{Ag}^+$ ionic pair [29]. Its presence in the sample TMAg-50 could be produced by the lack of coordination of Ag^+ ions by pyridine molecules after the drying process. As the temperature of densifying treatment increases to 200 °C (sample TMAg-200), a

whole dissociation of silver nitrate takes place and only the bands corresponding to “free” nitrate ions remain at 1367 and 1394 cm^{-1} , as observed previously [30–32]. Besides completing the silver–nitrate dissociation, related to the silver nanoparticles growth, the band of Si–OH groups, at 948 cm^{-1} , increases at expenses of the band corresponding to non-bridging oxygen at 909 cm^{-1} . The bands of the Si–O–Si network remain almost unaffected, i.e., disappearance of neither cyclosiloxanes nor smaller silica clusters is clearly absent.

Silver nanoparticles produce a clearly observable plasmonic band in the UV–visible spectra. Both position and intensity could be related to size and amount of silver nanoparticles, respectively, but a better technique to determine size particles like dynamic light scattering (DLS) or zeta potential using a particle sizer is needed to check the results observed by UV–visible spectroscopy. Fig. 2 reveals the evolution of silver nanoparticles developed in TMA samples as a function of the temperature of thermal treatment. The spectrum of the silver-free sample, TM-200, is presented as reference, where no plasmonic band is present. A clear evolution of silver nanoparticles is observed through the growth of the plasmonic band as the temperature of thermal treatment increases. In sample TMAg-50 an early-developed plasmonic band, with its maximum around 420 nm, is resolved. As temperature arises, such silver nanoparticles grow-up at expenses of the smaller silver clusters and ions. This feature is manifested both by an increase of the intensity and by a shift and widening of the plasmonic band. With treatments at 100 and 200 °C the maximum shifts to 470 nm and a shoulder remains at 420 nm (TMAg-100 and TMAg-200 samples). Although those maxima correspond to particles around 50 and more than 70 nm diameter [33], the spectra also could reflect the production of an extremely wide size distribution as a consequence of destabilization of Ag^+ ions.

It is well known that Porod's Law deals with biphasic systems with sharp interfaces between two different electron densities. This is usually applied to nanostructured materials such as nanoporous solids, nanocrystals or disordered nanoclusters embedded in solid or liquid matrices. SAXS curves of TM samples, Fig. 3a, show the presence of a well-defined Porod's Law at the lower values of q . Although the Guinier region is not observed under our experimental setup, the presence of a near q^{-4} decay without oscillations, characteristic of narrow size distributions, is a clear indication of development of polydisperse structures with smooth surfaces. This is a common characteristic of sol–gel materials as result of the existence of nanoporosity [34–36]. In acid catalyzed sol–gel materials, the resulting structure develops from the hydrolytic condensation of chemical precursors producing, at the beginning, small silica clusters, siloxane rings and higher fractal-like particles that afterwards will constitute the consolidated material. Comparing the

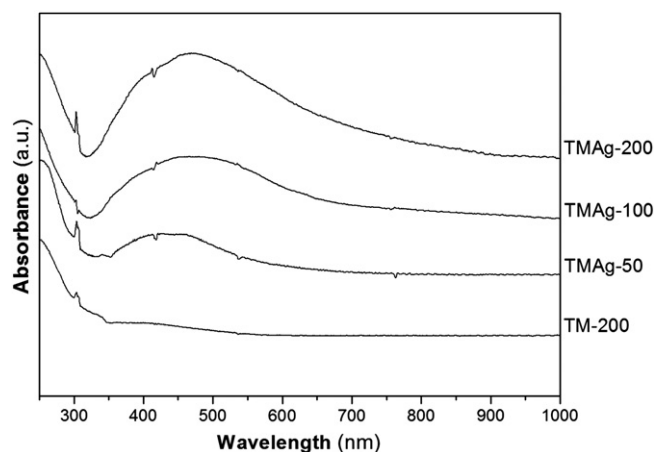


Fig. 2. Thermal evolution of the plasmonic band in UV–visible spectra of TMAg samples. Non doped TM sample treated at 200 °C is presented as reference.

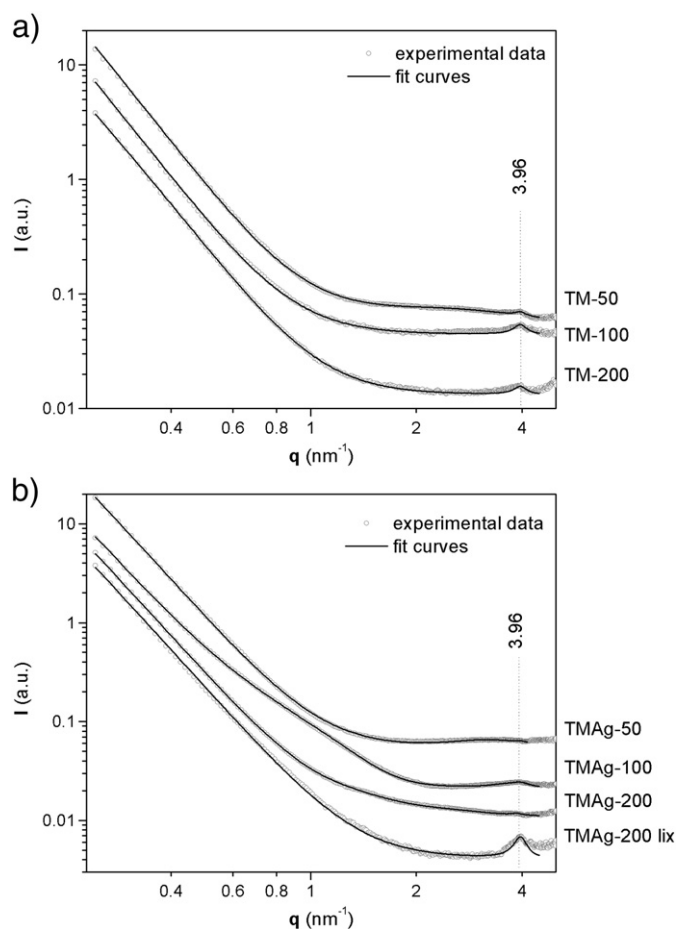


Fig. 3. SAXS curves obtained for a) TM and b) TMAg coatings as a function of thermal treatment and TMAg coating treated at 200 °C and lixiviated for 140 h in deionized water.

SAXS curves of the TM sample dried at 50 °C with the ones treated at 100 and 200 °C a clear difference is observed in the region of the higher q values, where the smaller components have a higher contribution to the X ray scattering [37]. Since no particles are added with the starter reagents, this behavior is attributed to the presence of the smallest constituent particles developed from the hydrolytic condensation of alkoxydes which, because of the increase of the crosslinking density with thermal treatments, consolidate with the bulk material and are only seen in TM-50 sample. The fit procedure of SAXS curve for TM-50 sample gives a size of 0.7 nm diameter for those smaller structures, which is certainly coincident with the characteristic size of cyclosiloxanes [38].

Independently of the densifying temperature, in every one of the studied samples, a single broad peak was observed at $q = 3.96 \text{ nm}^{-1}$. The position of this peak is associated to a characteristic length given by $2\pi/q_{\text{max}} = 1.6 \text{ nm}$. This feature is commonly observed in microemulsions and spinodal structures [39–41]. In the case of hybrid sol–gel materials, this phenomenon could also be explained by a spinodal-like phase separation between silica-rich and organic-rich domains resulting in a narrow pore size distribution of the silica network [42,43,21]. Although such spinodal-like structure should be present from the initial stages of gelling, in TM-50 sample the peak at 3.96 nm^{-1} is partially overlapped with the scattering of the smaller constitutive units.

SAXS curves of TMAg samples, Fig. 3b, suggest, in the higher q values, a strong presence of sub-nanometric particles. This kind of particles is clearly observable through high energy accelerators [44]. Certainly, the curves fitting evidence the presence of particles with 0.3 nm radius

whose intensity diminishes strongly from TMAg-50 to TMAg-100, were larger nanoparticles, of $1.85 \pm 0.21 \text{ nm}$ radius, are developed and a wide shoulder around 1 nm^{-1} appears in the SAXS curve. When sample is treated at 200 °C, the modeling yields only the presence of particles of 0.88 nm radius. The higher nanoparticles are not observable under our experimental set-up of SAXS.

The evolution of silver nanoparticles inside the hybrid matrix, evidently, starts with a nucleation and growth process from the ions. By effect of the thermal treatment, the possible mechanism responsible for the ripening process is the Ostwald ripening. As silver particles growth, its mobility is gradually diminished until they remain entrapped in the covalently bonded network. So, the particle migration and coalescence process turn in a non probable mechanism to promote further growth of silver particles.

3.2. Silver release and bactericidal behavior of hybrid films

The SAXS curve of the sample treated at 200 °C and exposed to a lixiviation process of 1 week immersion in deionized water, named TMAg-200 lix, is also showed in Fig. 3b, where a strong diminution in the higher q values allowed the peak at 3.96 nm^{-1} to get clearly visible. Immersion of TMAg samples in water produces a release of the smallest particles, as silver clusters and ions and the silica particles not consolidated to the hybrid matrix. In this process only the higher silver nanoparticles should remain entrapped inside the network of the hybrid coating.

Then, the performed structural analysis allows us to assume a rather complex scenario of a widely polydisperse silver particles embedded in a spinodal-like hybrid matrix with a well-defined characteristic dimension, as synchrotron SAXS experiments revealed. Such structural conformation makes the hybrid matrix of the sol–gel coating a size-selective membrane contributing to the confinement of the higher silver nanoparticles and the release of the smallest clusters and silver ions that are able to migrate throughout its structure, whose channels could act as a pathway. This phenomenon has a strong meaning on the performance of silver doped materials as bactericidal coatings. As the formation of silver nanoparticles is reduced, the availability of silver ions and clusters to provide the bactericidal activity is increased. Thus, the efficiency of silver doping could be defined in terms of non-confined, or releasable, silver. Another key factor, regarding to the coating performance, is the silver release rate, which is related to the life time of such materials.

Fig. 4 shows the cumulative silver release of TMAg samples at 1, 24 and 140 h immersions in deionized water at 30 °C. Although these experiments were made in conditions that are far from conditions for which these coatings were designed, they allow determining the

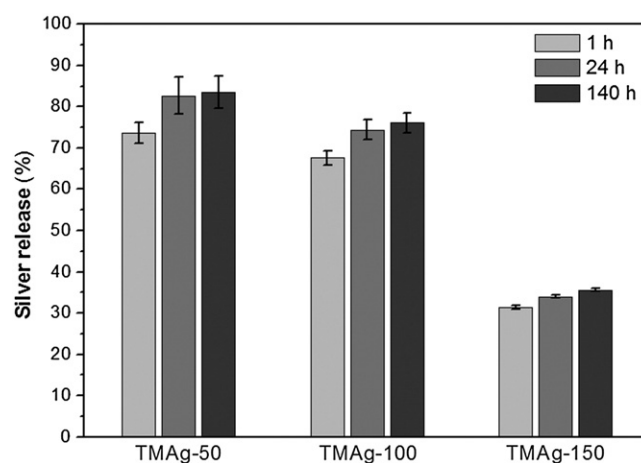


Fig. 4. Bar representation of silver release for TMAg samples immersed 1, 24 and 140 h in deionized water at 30 °C.

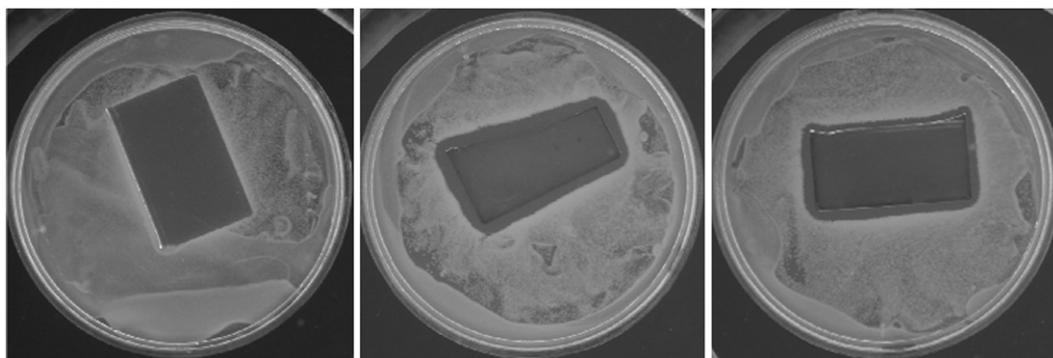


Fig. 5. Inhibition halo experiments on Petri dishes: a) TM-150 sample, b) TMAg-50 sample and c) TMAg-150 sample. Picture sizes: 5.8 cm.

influence of the processing parameters on the silver releasing behavior. Therefore, if we consider the releasing at 140 h immersion as an approximation to the maximum amount of releasable silver for a given sample, then two features could be clearly observed: a) for each sample, near the 90% of the releasable silver is lixiviated within the first hour of immersion, and b) the efficiency of the silver doping is, approximately, of 83, 76 and 36% for TMAg-50, TMAg-100 and TMAg-150 samples, respectively. These results are alike to those obtained by Mahltig et al. [45] and Stobie et al. [46] for different sol–gel coatings densified at similar temperatures to the ones analyzed in this work. Although a high releasing rate of the active agent could be useful in order to provide an intensive treatment, decreasing the possibility of resistant pathogens growth, this trend is contrary to purposes of long-term bactericidal coatings. Therefore, on the way to control the diffusive processes, some alternatives should be analyzed. The handling of the structural parameters, as porosity, crosslinking density, or the incorporation of denser nanoparticles, able to offer an obstacle to the diffusion of silver ions, are parameters compatible with the sol–gel process that could help in this sense.

Agar diffusion tests on *Escherichia coli*, were performed with TM and TMAg samples. A tight correlation between the inhibition halos and the amount of releasable silver was observed. Fig. 5a) at left displays the photograph corresponding to TM-150 sample, as expected, due to the absence of the bactericidal agent, no inhibition halo was observed. No inhibition halo was observed for the TM-150 sample, as expected due to the absence of bactericidal agent (Fig. 5a). For samples TMAg-50 and TMAg-150 (Fig. 5b) at center and 5c) at right respectively clear inhibition halos were obtained, being the biggest one the corresponding to the TMAg-50 sample.

Considering that only the smaller clusters and silver ions, which are the active components against microorganisms, could be released from coatings, the obtained microbiologic results are in accordance with the results obtained by structural analysis. Several authors have found a tight relationship between the size of silver nanoparticles and its behavior against microorganisms [47–50], on the basis of the smaller particles contributing a higher surface area to interact with bacteria.

4. Conclusions

Hybrid organic–inorganic sol–gel coatings were synthesized from the hydrolytic condensation of TEOS and MTES in acidic media, and doped with silver ions during the sol state by addition of a pyridine-stabilization alcoholic solution. From spectroscopic studies performed through ATR-FTIR, the effect of silver doping on the silica structure by stabilization of cyclosiloxanes and Si–OH groups up to 200 °C was determined, while the matrix structure was analyzed by synchrotron SAXS experiments which revealed the presence of a thermally stable spinodal-like structure of the hybrid matrix whose characteristic length, of 1.6 nm, remains unchanged with silver doping and thermal treatment.

As temperature of the thermal treatment rises, silver nanoparticles grow-up at expenses of the smaller clusters and Ag^+ ions, producing a partial confinement of silver in the matrix and a subsequent decrease of the doping efficiency.

Finally, the bacteriologic tests verified both the migration of silver to the surface of the material and the activity of silver coatings against *E. coli* cultures.

Acknowledgments

Authors want to acknowledge the Argentine National Council of Scientific and Technical Researches (CONICET), the Argentine National Agency of Scientific and Technological Promotion (ANPCyT PICT-2011-0938) and the National Synchrotron Light Laboratory, Campinas, Brazil (LNLS, Project 6780/10, proposal D11A-SAXS1-11517) for the financial supports. Also “Fundación Bunge y Born” is gratefully acknowledged for the postdoctoral grant of Dr Raul Procaccini. Finally, the financial support from EULA-NET (FP7-PEOPLE-2011-295197) project is also acknowledged.

References

- [1] S.A. Jones, P.G. Bowler, M. Walker, D. Parsons, Wound Repair Regen. 123 (2004) 288.
- [2] S. Silver, L.T. Phung, Annu. Rev. Microbiol. 50 (1996) 753.
- [3] J.H. Crabtree, R.J. Burchette, R.A. Siddiqi, I.T. Huen, L.L. Handott, A. Fishman, Perit. Dial. Int. 23 (2003) 368.
- [4] G. Zhao, S.E. Stevens Jr., Biomaterials 11 (1998) 27.
- [5] Y. Ando, H. Miyamoto, I. Noda, N. Sakurai, T. Akiyama, Y. Yonekura, T. Shimazaki, M. Miyazaki, M. Mawatari, T. Hotokebuchi, Mater. Sci. Eng. C 30 (2010) 175.
- [6] A.M. El-Kady, A.F. Ali, R.A. Rizk, M.M. Ahmed, Ceram. Int. 38 (2012) 177.
- [7] M.E. Rupp, T. Fitzgerald, N. Marion, V. Helget, S. Puumala, J.R. Anderson, P.D. Fey, Am. J. Infect. Control 32 (2004) 445.
- [8] F. Furno, K.S. Morley, B. Wong, B.L. Sharp, P.L. Arnold, S.M. Howdle, R. Bayston, P.D. Brown, P.D. Winship, H.J.J. Reid, J. Antimicrob. Chemother. 54 (2004) 1019.
- [9] E. Falletta, M. Bonini, E. Fratini, Nostro A. Lo, G. Pesavento, A. Becheri, Nostro P. Lo, P. Canton, P. Baglioni, J. Phys. Chem. C 112 (2008) 11758.
- [10] C.J. Brinker, G.W. Scherer, Sol–gel Science: The Physics and Chemistry of Sol–gel Processing, Academic Press, San Diego, California, USA, 1989.
- [11] A.B.G. Lansdown, J. Wound Care 11 (2002) 125.
- [12] R. Reisfeld, T. Saraidarov, V. Levchenko, J. Sol–Gel Sci. Technol. 50 (2009) 194.
- [13] R. Procaccini, S. Ceré, S. Pellice, Surf. Coat. Technol. 205 (2011) 5464.
- [14] T.C. Huang, H. Toraya, T.N. Blanton, Y. Wu, J. Appl. Crystallogr. 26 (1993) 180.
- [15] A.P. Hammersley, Scientific Software FIT2D, European Synchrotron Research Facility, Grenoble, 2009. (URL, <http://www.esrf.eu/computing/scientific/FIT2D/>).
- [16] R.M. Almeida, C.G. Pantano, J. Appl. Phys. 68 (1990) 4225.
- [17] J. Gallardo, A. Durán, D. Di Martino, R.M. Almeida, J. Non-Cryst. Solids 298 (2002) 219.
- [18] A. Fidalgo, L.M. Ilharco, J. Non-Cryst. Solids 283 (2001) 144.
- [19] Z. Sassi, J.C. Bureau, A. Bakkali, Vib. Spectrosc. 28 (2002) 299.
- [20] M. Nocun, K. Cholewa-Kowalska, M. Łaczka, J. Mol. Struct. 938 (2009) 24.
- [21] L.V. Ng, P. Thompson, J. Sanchez, C.W. Macosko, A.V. McCormick, Macromolecules 28 (1995) 6471.
- [22] S.A. Pellice, R.J.J. Williams, I. Sobrados, J. Sanz, Y. Castro, M. Aparicio, A. Durán, J. Mater. Chem. 16 (2006) 3318.
- [23] S. Yu, T.K.S. Wong, X. Hu, T.K. Goh, Thin Solid Films 462–463 (2004) 306.
- [24] A. Jitianu, A. Britchi, C. Deleanu, V. Badescu, M. Zaharescu, J. Non-Cryst. Solids 319 (2003) 263.
- [25] L.D. Ou, A.B. Seddon, J. Non-Cryst. Solids 210 (1997) 187.
- [26] A. Chmel, E.K. Mazurina, V.S. Shashkin, J. Non-Cryst. Solids 122 (1990) 285.

- [27] C. Carteret, *Spectrochim. Acta A* 64 (2006) 670.
- [28] G. De, A. Licciulli, C. Massaro, L. Tapfer, M. Catalano, G. Battaglin, C. Meneghini, P. Mazzoldi, *J. Non-Cryst. Solids* 194 (1996) 225.
- [29] G.J. Jam, M.J. Tait, J. Meier, *J. Phys. Chem.* 71 (1967) 963.
- [30] T.G. Chang, D.E. Irish, *J. Solution Chem.* 3 (1974) 175.
- [31] S. Pal, G. De, *Mater. Res. Bull.* 44 (2009) 355.
- [32] N. Satyanarayana, X. Xie, B. Rambabu, *Mater. Sci. Eng. B* 72 (2000) 7.
- [33] K.G. Stamplecoskie, J.C. Scaiano, V.S. Tiwari, H. Anis, *J. Phys. Chem. C* 115 (2011) 1403.
- [34] T.K. Goh, T.K.S. Wong, *Microelectron. Eng.* 75 (2004) 330.
- [35] T. Steriotis, E. Kikkinides, M. Kainourgiakis, A. Stubos, J.D.F. Ramsay, *Colloids Surf. A* 241 (2004) 231.
- [36] C. Scherdel, G. Reichenauer, *Microporous Mesoporous Mater.* 126 (2009) 133.
- [37] D.A. Donatti, Ruiz A. Ibañez, D.R. Vollet, *J. Non-Cryst. Solids* 292 (2001) 44.
- [38] B.C. Chakoumakos, R.J. Hill, G.V. Gibbs, *Am. Mineral.* 66 (1981) 1237.
- [39] K.V. Schubert, R. Strey, S.R. Kline, E.W. Kaler, *J. Chem. Phys.* 101 (1994) 5343.
- [40] S. Peng, Q. Guo, T.C. Hughes, P.G. Hartley, *Macromolecules* 44 (2011) 3007.
- [41] C.J. Gommès, S. Blacher, B. Goderis, J.P. Pirard, *Nucl. Instr. Meth. B* 238 (2005) 141.
- [42] C. Gommès, S. Blacher, B. Goderis, R. Pirard, B. Heinrichs, C. Alié, J.P. Pirard, *J. Phys. Chem. B* 108 (2004) 8983.
- [43] C.J. Gommès, B. Goderis, J.P. Pirard, S. Blacher, *J. Non-Cryst. Solids* 353 (2007) 2495.
- [44] M. Harada, Y. Kimura, K. Saijo, T. Ogawa, S. Isoda, *J. Colloid Interface Sci.* 339 (2009) 373.
- [45] B. Mahltig, D. Fiedler, H. Böttcher, *J. Sol-Gel Sci. Technol.* 32 (2004) 219.
- [46] N. Stobie, B. Duffy, D.E. McCormack, J. Colreavy, M. Hidalgo, P. McHale, S.J. Hinder, *Biomaterials* 29 (2008) 963.
- [47] M. Rai, A. Yadav, A. Gade, *Biotechnol. Adv.* 27 (2009) 76.
- [48] J.R. Morones, J.L. Elechiguerra, A. Camacho, K. Holt, J.B. Kouri, Ramírez J. Tapia, M.J. Yacaman, *Nanotechnology* 16 (2005) 2346.
- [49] V. Dal Lago, L. França de Oliveira, K. de Almeida Gonçalves, J. Kobarg, M. Borba Cardoso, *J. Mater. Chem.* 21 (2011) 12267.
- [50] G.A. Martínez-Castañón, N. Niño-Martínez, F. Martínez-Gutierrez, J.R. Martínez-Mendoza, F. Ruiz, *J. Nanopart. Res.* 10 (2008) 1343.